SCIENCE CHINA
Technological Sciences

•Article•

August 2024 Vol.67 No.8: 2515–2529
https://doi.org/10.1007/s11431-023-2632-9

Empirical model of concrete block fragment behavior under explosion loads

YANG Shuai, NING JianGuo, REN HuiLan & XU XiangZhao*

State Key Laboratory of Explosion Science and Safety Protection, Beijing Institute of Technology, Beijing 100081, China

Received December 8, 2023; accepted March 6, 2024; published online July 30, 2024

Concrete structures undergo integral fragmentation under explosion loads. The fragmentation degree and particle-size distribution of concrete blocks under explosion loads must be considered during mining to ensure safety. In this study, the impulse is calculated based on the relationship between overpressure and time, and the impact energy of the explosion wave is obtained based on blast theory. Subsequently, the Mohr-Coulomb shear strength fracture criterion is introduced to determine the ultimate shear stress of the concrete materials, and an empirical model that can effectively calculate the energy consumption of concrete blocks under explosion loads is established. Furthermore, concrete fragments with different particle sizes under explosion scenarios are quantitatively predicted with the principle of energy conservation. Finally, explosion tests with different top standoff distances are conducted, and the concrete fragments after the explosion tests are recovered, sieved, weighed, and counted to obtain experimental data. The effectiveness of the fragment empirical model is verified by comparing the model calculation results with the experimental data. The proposed model can be used as a reference for civil blasting, protective engineering design, and explosion-damage assessment.

concrete structures, explosion loads, fragment behavior, empirical model

Citation: Yang S, Ning J G, Ren H L, et al. Empirical model of concrete block fragment behavior under explosion loads. Sci China Tech Sci, 2024, 67: 2515–2529, https://doi.org/10.1007/s11431-023-2632-9

1 Introduction

Concrete engineering structures are highly susceptible to explosion loads during service, and predicting the fragment behavior of concrete structures under explosion loads is challenging. The explosive detonation process generates a significant amount of energy that can be rationally utilized in daily production. The fragmentation of brittle materials under explosion loads is ubiquitous in fields that entail the mining of rocky minerals [1], the splitting and fragmentation of coal blocks [2], and the demolition of abandoned buildings [3]. The fragmentation of concrete materials is widely investigated in the field of rock blasting and safety protection; furthermore, it is an important indicator in water conservancy and hydropower, construction transportation, and mineral exploitation projects. Therefore, an empirical calculation model for fragments of concrete materials under explosion loads must be established to promote blasting technology, as it can reveal the fragmentation mechanism of brittle materials and improve the quality and efficiency of engineering.

The fragmentation of concrete blocks under explosion loads is extremely complex; it involves the propagation and attenuation of the explosion wave, the reflection, and enhancement of the stress wave, the stress concentration and energy dissipation of the material, as well as the escape of high-pressure explosion gas products. The typical methods for calculating explosion energy in the current study are indirect-calculation and empirical-formula calculation methods.

The indirect-calculation method is primarily used to measure the deformation degree, damage area, and other

*Corresponding author (email: xzxu@bit.edu.cn)

parameter information that can reflect the energy absorption of the target [4–7]; subsequently, the information from these parameters is used to indirectly convert the initial explosion energy. However, this method is susceptible to significant measurement errors, and the energy dissipation in each physical process cannot be comprehensively considered in the conversion calculation; thus, the calculation results yielded by this method are generally unsatisfactory. Various types of sensors are installed at the target to obtain more accurate energy signals [8,9]; subsequently, the calculation is performed based on the loading signals to compensate for the significant measurement errors in indirect calculations. This method is applied extensively in explosion tests involving small charges and low strain rates. However, as the charge mass and loading rate increase, the integrity of the sensor may not be guaranteed in strong impact experiments, and the test data acquired by the sensor are extremely volatile, thus rendering the effective capture of explosion-load data difficult to achieve [10,11]. Moreover, the indirect-calculation method is only applicable to specific explosion scenarios and can not be used to predict results under unknown explosion conditions. Accordingly, the empirical-formula calculation method is applied to quantify explosion; it involves fitting the existing experimental data as well as summarizing and generalizing the empirical formula corresponding to the explosion conditions. Moreover, the empirical formula can be used to calculate the parameter information in unknown explosion scenarios [12–16]. However, effective empirical formulas require a significant amount of experimental data, and the applicability of these formulas is limited. Hence, an empirical model with significant engineering value that can rapidly calculate the initial explosion energy was established.

Concrete structures are susceptible to compression, deformation, fragmentation, loosening, and throwing under explosion loads [17–22]. This process has been investigated extensively, and many have concluded the fragments of concrete structures under explosion loads are caused by explosion waves and gas products generated by explosion [23–27]. However, the fragmentation of nonhomogeneous materials such as concrete is primarily due to the explosion wave, particularly in explosion scenarios involving a stand-off distance. The expansion pressure of the gas products is small, which only accelerates the separation of fragments, whereas the explosion wave possesses a high amount of initial energy, which perturbs the concrete material significantly and fragments the structure.

Studies pertaining to the fragment behavior of concrete-like materials subjected to strong impact loads are primarily based on elasticity, fracture, damage, and fractal damage theories [28–32]. Based on the elasticity theory, concrete materials are in the elastic deformation stage before fragmentation, which facilitates the simplification of the force process of the material without considering the initial defects and irreversible damage of the material; consequently, the calculation results obtained based on this theory are inconsistent with the actual situation. Meanwhile, fracture theory considers the effect of internal microcracks in concrete materials based on elasticity theory and states that the fragmentation of concrete materials is due to the expansion of internal microcracks [33–35]; however, this theory does not provide an analysis and description of the material-deterioration process, which limits its application scope. Damage theory correlates the activation number of internal microcracks in concrete materials with the damage degree of the structure; moreover, a damage factor is introduced to characterize the changes in the mechanical properties of the material. However, a generalized construction of the damage factor has not yet been established, and numerous basic material parameters must be considered comprehensively when the damage factor is introduced, thus limiting the wide application of damage theory. Fractal damage theory introduces the concept of fractal geometry into studies pertaining to the dynamic properties of concrete materials and uses the fractal dimension as the main parameter to characterize the damage degree of concrete materials [36–38], thus providing a basis for the construction of damage factors. However, obtaining the key parameters of the fractal dimension is challenging, particularly when the concrete material is subjected to explosion loads. Currently, this parameter is primarily obtained experimentally; thus, reasonable experimental techniques to obtain the effective fragment parameters of concrete materials should be prioritized. Currently, the experimental methods for obtaining the parameter information of concrete fragments include three-dimensional (3D) scanning, image-recognition, and sieve statistics methods [39–42]. Nevertheless, these methods require unique experimental equipment and analysis software; furthermore, their efficiency and accuracy are unsatisfactory when used in cases involving a significant amount of parameter information pertaining to concrete fragments.

The fragment empirical model is an effective method for calculating the fragment behavior of concrete structures under strong impact loads. Ref. [41] investigated the fragmentation behavior of concrete using sieve analysis, but the fracture criterion was not sufficiently involved in this research process. Concrete structures are bound to fragments under explosion loads, and appropriate fracture criteria must be selected to describe such phenomena reasonably. The existing fracture criterion is proposed from the aspects of stress, strain, and energy, and the fracture criterion based on the stress and strain perspective is more intuitive; thus, it has been applied to most scenarios [43–45]. The typical fracture criteria include the Tresca-Mises, Drucker-Prager, and Mohr-Coulomb criteria. The Tresca fracture criterion is excellent for characterizing the damage of a single shear plane of a material, whereas the Mises fracture criterion fully

considers the shear stress on the octahedron of a material. These two fracture criteria have been used primarily for the damage and fracture prediction of metals, whereas they are unsuitable for brittle materials. The Drucker-Prager fracture criterion couples the effects of friction and characterizes the volume expansion when materials are loaded. Nevertheless, it is derived from the Mohr-Coulomb fracture criterion for the plane strain. The Mohr-Coulomb fracture criterion considers the effects of compressive strength, the friction of particles inside a material, the water content of a material, and the history of loads; hence, it is applicable to brittle materials with a compressive strength much higher than the tensile strength. In fact, it is widely used to describe the mechanical properties of brittle materials such as concrete and rocks [46]. The fragment behavior of concrete structures subjected to explosion loads is typically determined by the external loads on the structure, which exceed the shear limit of the material itself; hence, the Mohr-Coulomb fracture criterion is coupled with the empirical model to characterize the fracture mechanism of concrete blocks under explosion loads. Moreover, the strain from shear stress is used to calculate the fragmentation energy, which is included in the empirical model for concrete fragmentation.

In this research, the loading characteristics of explosion waves are analyzed, the impulse is calculated based on the relationship between overpressure and time, and the effective impact energy of the explosion wave is obtained based on blast theory. Subsequently, the Mohr-Coulomb shear strength fracture criterion is introduced to determine the ultimate shear stress of concrete materials, and an empirical model is established by combining this fracture criterion. Additionally, concrete fragments with various diameter sizes in an explosion scenario are quantitatively predicted with the principle of energy conservation. Finally, the explosive was used to carry out the explosion test at various top spacing distances, furthermore, the concrete fragments resulting from the tests were collected and recycled fragments were further sieved with a variety of screen sizes. The sieved concrete fragments are subjected to weighing and counting to obtain experimental data on fragments of various particle sizes. The effectiveness of the fragment empirical model is demonstrated by contrasting the model calculation results with the experimental data. The fragmentation process of the concrete-resembling material and its energy-consuming behavior during the load-bearing period can be explained by this empirical model, thus benefitting the development of blasting technology and the design of protection engineering.

2 Calculation of explosion energy

A charge explosion is a complex and rapid process that releases significant amounts of thermal energy and generates high-pressure explosion gas products. The static medium in air is perturbed by the gas products and the media state parameters are changed. Compression waves propagating in all directions are generated in space and these compression waves are superimposed repeatedly to form the initial explosion wave. An extremely high initial energy is borne by the explosion wave in the form of a wavefront that continues to propagate outward. The wavefront surface continues to expand during the propagation process, whereas the shockwave energy attenuates gradually. Effectively calculating the explosion energy in different explosion scenarios is crucial for the assessment of explosion hazards and the design of protective engineering.

2.1 Propagation of explosion wave

Explosion energy can be classified into two categories: full work and local work. Full work involves a certain distance from the detonation source and is closely related to the release of all energy, whereas local work is determined by the burst pressure on the surface of the explosion wave. The explosion work depends on the initial energy of the explosion wave when the concrete block from the explosion source is at a certain interval distance. The overpressure-time relationship for an explosion wave in air is shown in Figure 1.

As shown in Figure 1, the explosion wave overpressure zone can be partitioned into positive- and negative-pressure zones. The positive-pressure zone within the shockwave overpressure comprises upward and downward phases. The explosion wave required a duration of T_1 to reach the concrete block, at which time the shockwave overpressure from the original atmospheric pressure P_0 required a duration of T_2 to reach the peak overpressure P_m. As the explosion progressed, the surface of the shockwave front passed through the concrete block, at which point the overpressure of the shockwave block decreased rapidly. Subsequently, after T_3, the initial value of the atmospheric pressure attenuated exponentially. The units for time and pressure used herein are s

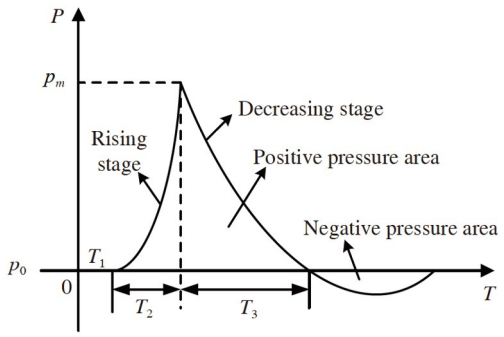

Figure 1 Relationship between blast wave overpressure and time after blast occurs in air. Blast-wave overpressure zone is partitioned into positive-pressure zone (pressure > 0) and negative-pressure zones (pressure < 0).

and MPa, respectively. A negative-pressure zone appeared as the shockwave overpressure continued to decrease, and the negative-pressure peak gradually returned to the atmospheric pressure. The peak overpressure of the explosion wave is calculated as follows [47]:

$$\overline{R} = M^{1/3}/H, \tag{1}$$

$$P_m = -0.0197\overline{R}^3 + 0.3133\overline{R}^2 + 3.8109\overline{R} - 4.0715 \quad (1 \leqslant \overline{R} \leqslant 12), \tag{2}$$

where M is the mass of the charge (kg), H is the stand-off distance (m), and R is the scale distance ($kg^{1/3}$/m). The time required by the explosion wave to reach the concrete block, the duration of the shock-wave overpressure rising phase, and the duration of the falling phase can be calculated as follows, respectively [48]:

$$T_1 = 0.34M^{-0.2}H^{1.4}/C, \tag{3}$$

$$T_2 = 0.0019H^{1.3}/M^{0.43}, \tag{4}$$

$$T_3 = 0.0005H^{0.72}M^{0.16}, \tag{5}$$

where C is the speed of sound propagation in air (340 m/s).

The overpressure value of the blast wave changes with the propagation time and the movement positions, and this functional relation of the shockwave overpressure value at different times and positions is as follows:

$$P(T,H) = \frac{526.3P_mTH^{-1.3}}{M^{-0.43}} \quad (0 \leqslant T \leqslant T_2), \tag{6}$$

$$P(T,H) = \left[P_m - (T-T_2)P_m/T_3\right]^{-a(T-T_2)/T_3} \quad (T_2 \leqslant T), \tag{7}$$

where a is a constant that controls the decay rate of the overpressure of the explosion wave, which can be calculated as follows:

$$a = 1.62P_m^{0.3} + \left(5.13P_m^{0.28}\right)^{-1.05P_m^{0.37}(T-T_2)/T_3}. \tag{8}$$

2.2 Calculation of energy exerting on concrete block

The positive-pressure zone is the main source of energy for a concrete block under explosion loads; hence, the parameters in the positive-pressure zone are calculated, and information regarding the overpressure and time of the explosion wave is obtained. Furthermore, the fragmentation effect of concrete blocks is affected by the shock wave overpressure and the impulse is relatively large; thus, these effects are comprehensively considered in the calculation of the impact energy. The propagation of explosion waves in air is complex. Therefore, the following assumptions are introduced to calculate the impact energy.

(1) The instantaneous explosion of the explosive detonation is adiabatic.

(2) The radiation energy, light energy, acoustic energy loss, and viscous friction caused by energy dissipation are disregarded during the detonation of explosives.

(3) The energy distribution of the explosion wave during the propagation process is uniform throughout the wavefront.

(4) The shock wave energy acting on the concrete block is assumed to originate primarily from the positive pressure region, and the negative pressure region is disregarded.

(5) The acceleration distance of the impact energy on the concrete fragments is minute in this study; thus, the influence of kinetic energy on the concrete fragments is neglected.

Moreover, the impulse and momentum changes in the rising and decreasing stage of the shockwave overpressure within the positive-pressure zone can be calculated separately based on the relationship between overpressure and time as follows:

$$T_+ = T_2 + T_3, \tag{9}$$

$$I_0 = I_R + I_D = \int_0^{T_+} P(T,H)\mathrm{d}T, \tag{10}$$

where T_+ denotes the duration of the positive pressure; I_0 denotes the impulse of the concrete block under explosion loads; and I_R and I_D denote the impulses of the rising and decreasing phases, respectively.

The explosion wave separates from the explosion products during an air explosion and propagates forward after the separation when the explosion products stop expanding. Figure 2 shows the distribution of the shock-wave overpressure at different locations over a wide range. Adiabatic compression and energy attenuation occur during the propagation of an explosion shockwave, and the energy loss

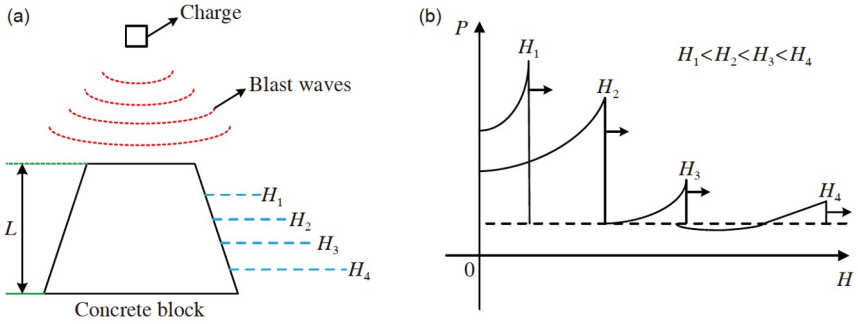

Figure 2 (Color online) The relationship between blast wave over-pressure and displacement after a blast in air. (a) Schematic illustration of the principle for a blast wave impacting the concrete block; (b) the attenuation of the over-pressure in the propagation direction.

during this propagation process is proportional to the intensity of the explosion wave. The explosion wave first arrives at the concrete block surface. As the shockwave front develops further, the block is subjected to impacts at different locations. Impulse is the cumulative effect of the impact force on the concrete block, and the impulse of the block is numerically equal to its momentum change. Different types of impulse waveforms are generated under different burst sources; thus, the damage effect at the concrete block differs significantly for the same impulse value. The length of the concrete block in the explosion-wavefront direction is denoted as L, and integration can be performed in the dimension direction to obtain the energy of the entire concrete block under explosion loads with the following formula:

$$E_0 = \int_0^H \int_0^{T_+} \frac{P^2(T,H)}{\rho_0 C} \mathrm{d}T \mathrm{d}L, \tag{11}$$

where E_0 denotes the impact energy of the concrete block under explosion loads, ρ_0 denotes the gas density, and C denotes the speed of sound.

3 Empirical model

Concrete structures under explosion loads experience different degrees of damage, and the degree of damage to the concrete structure is positively correlated with the strength of the explosion load. Compressive tests were first performed on concrete cube specimens to obtain the basic mechanical properties of the concrete materials, and the ultimate compressive strength and stress-strain relationship of the concrete materials were determined via several tests. Furthermore, the Mohr-Coulomb fracture criterion was introduced to describe the fragment behavior and fracture mechanism of the concrete materials, and the fragmentation energy of concrete materials was calculated according to this fracture criterion. Finally, a fragment empirical model with a coupled fracture criterion for a concrete block under explosion loads was established by combining the impact and ultimate deformation energies of the concrete block.

3.1 Mechanical properties tests

The mechanical properties of concrete materials were tested via compressive tests to establish an effective empirical model for the concrete blocks under explosion loads. The geometrical dimensions of the concrete specimens used in this study were 100 mm × 100 mm × 100 mm. The concrete specimens used in the tests were prepared from the same batch and contained the same constituent materials. The strength grade of the concrete specimens was C30. The concrete specimens were wrapped and sealed after pouring, and the batch of poured concrete were stored at the normal temperature room for curing.

Eight concrete specimens were selected for compressive tests. The eight concrete specimens were first sanded before the tests, and 2 mm strain gauges with 120 Ω resistance were fixed vertically on the surface. The pressure-bearing surfaces of the concrete specimens were coated with lubricating agent materials to minimize the influence of friction during the experimental process, and the eight concrete specimens were tested in compression with a material testing machine produced by Kexing Instruments, Inc., respectively. The experimental data were registered using sensors, the displacement rate was set to complete the loading of the concrete specimens in the tests. The strain gauges in the concrete specimens were connected to BZ2205C static resistance strain gauges, and the data of static resistance strain were observed after the test to obtain the strain condition of the concrete specimens. Figure 3 shows the stress-strain relationship of a 5# concrete specimen; the compressive strength of this concrete specimen was 31.87 MPa and the corresponding ultimate compressive strain value was approximately 0.0033, as shown in the figure. The average value of compressive strength of the concrete materials used in this study was 29.40 MPa, which was obtained after compressive tests were performed on eight concrete specimens of strength grade C30.

Concrete is a typical strain rate-sensitive material that exhibits different mechanical properties under different loads [49,50]. The compressive strength of concrete gradually in-

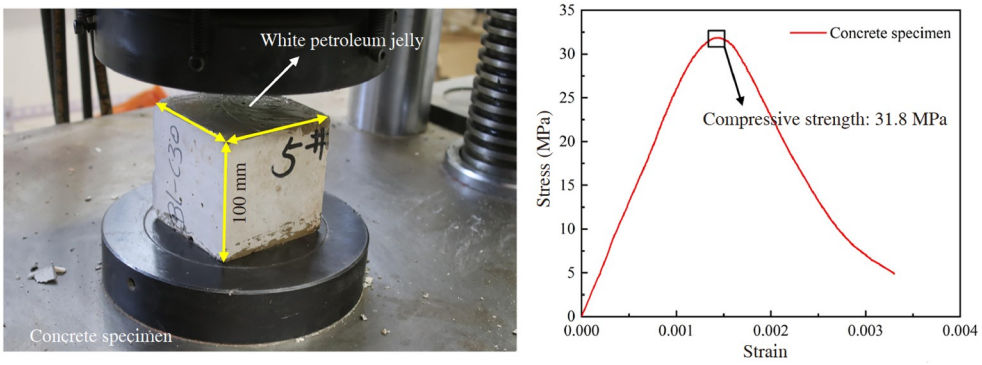

Figure 3 Stress-strain relationship of concrete specimen, test results of 5# concrete specimen are shown.

creases with the loading rate. The strain rate of a concrete material under explosion loads will be high because the duration of the blast process is short. In this study, a dynamic compressive strength enhancement factor DIF_c was introduced to characterize the compressive strength of a concrete block under explosion loads. The dynamic enhancement factor of concrete can be calculated as follows [51]:

$$\mathrm{DIF}_c = \begin{cases} \left(\dot{\varepsilon}/\dot{\varepsilon}_c\right)^{1.026\alpha_s}, & \dot{\varepsilon} \leqslant 30\ \mathrm{s}^{-1}, \\ \gamma_s\left(\dot{\varepsilon}/\dot{\varepsilon}_c\right)^{1/3}, & \dot{\varepsilon} > 30\ \mathrm{s}^{-1}, \end{cases} \tag{12}$$

$$\log\gamma_s = 6.156\alpha_s - 2, \tag{13}$$

$$\alpha_s = 1/\left(5 + 9f_c/f_{cm}\right), \tag{14}$$

where $\dot{\varepsilon}$ is the equivalent strain rate; $\dot{\varepsilon}_c$ is the strain rate in the static compression test; f_c is the static compressive strength; and f_{cm} is the reference strength, which was set as 10 MPa in this study.

$$\mathrm{DIF}_E = \left(\dot{\varepsilon}/\dot{\varepsilon}_c\right)^{0.026}, \tag{15}$$

$$\mathrm{DIF}_\varepsilon = \left(\dot{\varepsilon}/\dot{\varepsilon}_c\right)^{0.02}. \tag{16}$$

DIF_E and DIF_ε are the dynamic enhancement factors for the elastic modulus and ultimate strain of the concrete material, respectively.

3.2 Mohr-Coulomb fracture criterion

Concrete is a multi-component granular material that primarily depends on the friction between particles to withstand external loads. Damage to concrete materials is primarily caused by shear stresses, which result in a relative slip between the particles of the material. Shear damage formed under stress is considered in the Mohr-Coulomb fracture criterion, which describes the yielding and fracture behaviors of concrete materials using the maximum shear stress or a single shear stress. Moreover, the criterion integrates the influencing factors, such as the compressive strength between the internal microparticles of the material, the friction effect between multiple interfaces, the water content of the material, and the change in the historical process of external loading. Hence, this fracture criterion is applicable to brittle materials with compressive strengths much higher than tensile strengths, and it is widely used to describe the mechanical properties of concrete and rock materials. Therefore, the shear damage energy consumption of concrete materials was calculated based on this fracture criterion. The Mohr-Coulomb fracture criterion is expressed as [52]

$$\tau_m = c + \sigma_n\tan\varphi, \tag{17}$$

where τ_m is the ultimate shear stress of the concrete material; c is the cohesive force of the concrete, which is related to the material components, density, and moisture content; σ_n is the ultimate stress of the concrete material, which is calculated using the compressive strength and strength enhancement factor; and φ is the angle of internal friction, which is related to the initial porosity ratio of the concrete, the shape of the internal granules, the particle gradation, and the roughness of the granule surface. In this study, $c = 9.1$ MPa and $\varphi = 37°$ were used [53]. $\tan\varphi$ is the coefficient of internal friction and $\sigma_n\tan\varphi$ is the internal friction, which is affected by the loading rate.

3.3 Empirical model with coupled fracture criterion

The concrete material unit is damaged when the strain energy reaches the surface energy required to damage the unit; thus, the concrete block exhibits an integral fragmentation behavior when all concrete material units are damaged instantaneously. In this study, the energy associated with the failure of the concrete block unit E_τ is calculated as follows:

$$E_\tau = \int_0^{\varepsilon_\tau} \tau_m \mathrm{DIF}_\varepsilon \mathrm{d}\varepsilon, \tag{18}$$

where ε is the strain of the concrete material and ε_τ is the ultimate strain of the concrete material in the shear direction. The shear force from the Mohr-Coulomb fracture criterion is substituted into the above formula, which yields

$$E_\tau = \int_0^{\varepsilon_\tau} \left[c + 10^{\frac{-3.844f_{cm}-18f_c}{5f_{cm}+9f_c}} f_c\tan\varphi\left(\dot{\varepsilon}/\dot{\varepsilon}_c\right)^{1/3}\right] \cdot \left(\dot{\varepsilon}/\dot{\varepsilon}_c\right)^{0.02}\mathrm{d}\varepsilon. \tag{19}$$

The difference between the deformation and damage mechanisms of concrete and metal materials results in significant differences in the damage characteristics. Damage to metal materials is attributed to shear stress, which causes the crystalline structure to undergo slip damage; thus, material damage occurs under shear stress, and the angle between the damaged surface and the main stress surface is 45°. However, the deformation and damage of concrete materials are closely related to the law of friction, which causes the angle between the damaged surface of concrete materials and the main stress surface to change.

$$\theta = \frac{90° + \varphi}{2} = 45° + \frac{\varphi}{2}. \tag{20}$$

Therefore, the shear-damage energy consumption of a material unit under explosion loads can be calculated as follows:

$$E_\tau = \int_0^{\varepsilon_\tau} \frac{c\left(\dot{\varepsilon}/\dot{\varepsilon}_c\right)^{0.02} + 10^{\frac{-3.844f_{cm}-18f_c}{5f_{cm}+9f_c}} f_c\tan\varphi\left(\dot{\varepsilon}/\dot{\varepsilon}_c\right)^{-0.35}}{\cos\theta}\mathrm{d}\varepsilon. \tag{21}$$

In the present study, the quantity for concrete fragments at the corresponding diameter is assumed to be N_{R_i}. The integral energy consumption in the fragmentation process can be found by combining the shear-damage energy consump-

tion of a material unit under explosion loads.

$$E_f=\int_0^{\varepsilon_\tau}\frac{\sqrt{2}\,cN_{R_i}+\sqrt{2}\,N_{R_i}f_c\tan\varphi\left(\dot{\varepsilon}/\dot{\varepsilon}_c\right)^{1/3}\cdot 10^{\frac{-3.844f_{cm}-18f_c}{5f_{cm}+9f_c}}}{\left(\cos\frac{\varphi}{2}-\sin\frac{\varphi}{2}\right)\left(\dot{\varepsilon}/\dot{\varepsilon}_c\right)^{-0.02}}\mathrm{d}\varepsilon. \tag{22}$$

The concrete block deforms before it fragments. Block deformation is primarily attributed to the compression of the concrete material in the explosion-wave direction. The deformation of the material absorbs the external impact energy, and the deformation of the concrete block under explosion loads can be classified into shape deformation and volumetric deformation. The energy can be obtained from the strain energy density V_d associated with the shape deformation of the concrete material and the strain energy density V_v related to volume deformation.

$$V_d=\frac{\varepsilon^{0.641}f_c{}^2(1+\mu)}{6E\dot{\varepsilon}_c{}^{0.641}}\cdot 10^{\frac{-7.688f_{cm}-36f_c}{5f_{cm}+9f_c}}, \tag{23}$$

$$V_v=\frac{\varepsilon^{0.641}f_c{}^2(1-2\mu)}{6E\dot{\varepsilon}_c{}^{0.641}}\cdot 10^{\frac{-7.688f_{cm}-36f_c}{5f_{cm}+9f_c}}. \tag{24}$$

The energy absorbed by the deformation of a concrete block under explosion loads can be determined by using the dynamic enhancement factor and strain energy density as follows:

$$E_d=\int_0^V\frac{f_c^2(2-\mu)\cdot 10^{\frac{-7.688f_{cm}-36f_c}{5f_{cm}+9f_c}}}{6E\left(\dot{\varepsilon}/\dot{\varepsilon}_c\right)^{-0.641}}\mathrm{d}V, \tag{25}$$

where E_d denotes the deformation energy; V is the volume of the concrete block; and E and μ denote the modulus of elasticity and Poisson's ratio, respectively.

In this study, the initial energy of the charge was calculated based on the relationship between the overpressure and time, and an empirical model coupled with the Mohr-Coulomb fracture criterion was established to determine the fragment energy of the concrete block under explosion loads. The deformation energy consumption was obtained with the strain energy density. However, a fragment empirical model which could validly estimate the quantity for fragments at the corresponding diameter of concrete blocks under an explosion scenario requires further investigation into the energy-distribution relationship of concrete fragments with the corresponding particle sizes. The external energy on the concrete to carry out impact damage, will make massive, varying diameter sizes of the concrete fragments are formed, these fragments consume the majority of the energy carried by the explosion shock wave. Nevertheless, the weight of concrete fragments at a particular diameter M_{R_i} can be expressed as a function of the number of fragments N_{R_i}, the density of the concrete material ρ, and the characteristic particle size R_i:

$$M_{R_i}=f\left(N_{R_i},\rho,R_i\right). \tag{26}$$

The relationship between the mass distribution of the concrete fragments at a particular particle size can be expressed as follows:

$$f\left(M_{R_i}\right)=\frac{N_{R_i}\rho R_i^3}{M_c}, \tag{27}$$

where $f\left(M_{R_i}\right)$ is the mass of concrete fragments with a specific particle size and M_c is the mass of the recovered concrete fragments. Notably, the recovery rate of the fragments results in energy loss, and the recovery rate η decreases because the concrete material is inevitably pulverized under explosion loads.

$$\eta=\frac{M_c}{M}, \tag{28}$$

where M is the total mass of the concrete block. Therefore, the effective energy of the concrete fragments with a specific particle size $f\left(E_{R_i}\right)$ is

$$f\left(E_{R_i}\right)=f\left(M_{R_i}\right)\eta E_0. \tag{29}$$

That is

$$f\left(E_{R_i}\right)=\frac{N_{R_i}\rho R_i^3}{M}\int_0^H\int_0^{T_+}\frac{P^2(T,H)}{\rho_0 C}\mathrm{d}T\mathrm{d}L. \tag{30}$$

Consequently, a fragment empirical model of concrete can be established based on the principle of energy conservation.

$$\int_0^{\varepsilon_\tau}\frac{\sqrt{2}\,c\mathrm{DIF}_{\dot{\varepsilon}}N_{R_i}+\sqrt{2}\,N_{R_i}\mathrm{DIF}_{\dot{\varepsilon}}f_c\mathrm{DIF}_c\tan\varphi}{\cos\frac{\varphi}{2}-\sin\frac{\varphi}{2}}\mathrm{d}\varepsilon =f\left(E_{R_i}\right)-\int_0^V\frac{f_c^2(2-\mu)\mathrm{DIF}_c{}^2}{6\mathrm{DIF}_E E}\mathrm{d}V. \tag{31}$$

A fragment empirical model of a concrete block under explosion loads can be established by combining the analyses above as follows:

$$\sum_{i=1}^n\frac{N_{R_i}\rho R_i{}^3}{M}\int_0^H\int_0^{T_+}\frac{P^2(T,H)}{\rho_0 C}\mathrm{d}T\mathrm{d}L -\int_0^V\frac{f_c^2(2-\mu)\cdot 10^{\frac{-7.688f_{cm}-36f_c}{5f_{cm}+9f_c}}}{6E\left(\dot{\varepsilon}/\dot{\varepsilon}_c\right)^{-0.641}}\mathrm{d}V =\sum_{i=1}^n\int_0^{\varepsilon_\tau}\frac{\sqrt{2}\,cN_{R_i}+\sqrt{2}\,N_{R_i}f_c\tan\varphi\left(\dot{\varepsilon}/\dot{\varepsilon}_c\right)^{1/3}\cdot 10^{\frac{-3.844f_{cm}-18f_c}{5f_{cm}+9f_c}}}{\left(\cos\frac{\varphi}{2}-\sin\frac{\varphi}{2}\right)\left(\dot{\varepsilon}/\dot{\varepsilon}_c\right)^{-0.02}}\mathrm{d}\varepsilon. \tag{32}$$

4 Validation and prediction of the empirical model

Explosion tests were conducted with different top stand-off distances to validate the proposed empirical model. After performing the tests, the concrete fragments resulting from the explosion tests are collected and the recycled fragments are further sieved with a variety of screen sizes. The sieved concrete fragments are subjected to weighing and counting to obtain parameter data on fragments under various explosion conditions. The experimental data were compared with the calculation results of the present empirical model. Furthermore, the present empirical model was used to predict the fragmentation behavior of a concrete block under explosion loads.

4.1 Test setup

The charges used in the tests were sheet rectangular B-explosives, and the specific material parameters of the charges are listed in Table 1. The individual charge has a weight of 5 kg in the present experiment. The weight of the explosive was changed by superimposing individual charge to conveniently set a variety of explosive amounts under different experimental conditions for it to be used in the tests. The concrete blocks used in the explosion tests were poured into the same batch as the concrete specimens used in the compression tests to ensure that the concrete material exhibited consistent mechanical properties. The strength grade of the concrete block after curing was C30, and a schematic illustration of the concrete block with dimensions is shown in Figure 4. The material parameters of the concrete block are listed in Table 2.

The cured and molded concrete block was positioned horizontally at the location indicated, an aluminum alloy herringbone ladder was used in the experiment to suspend the charge. First, the aluminum alloy herringbone ladder was put up on the concrete block directly above, and the bottom end of the aluminum alloy herringbone ladder was fixed on the ground using steel pins. The safety net was sealed in a carton box with a charge suspended above the concrete block, and the height of the charge was controlled using the safety net. Electric detonators were used in the tests, the

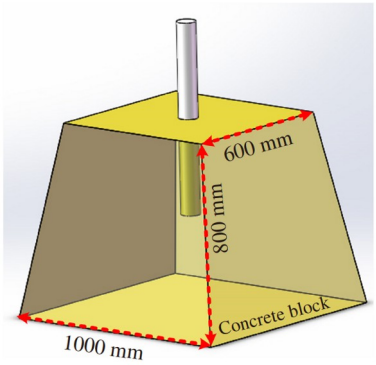

Figure 4 Schematic illustration of concrete block used in test (created using 3D modeling software).

electric detonators were also energized to achieve detonation of the charges. In this research, the explosion tests were performed thrice under a charge mass of 30 kg and the top spacing of 500, 750, and 950 mm. The test arrangement is presented in Figure 5.

4.2 Test results

4.2.1 Damage morphology of concrete blocks

The experimental process of the concrete block under the explosion load was photographed with a high-speed camera, as shown in Figure 6. A large flame was rapidly generated after detonation and the concrete block was encompassed. Both the concrete block and metal ladder shattered, and concrete fragments were formed under the high explosion energy. These fragments dispersed rapidly along the center of the detonation, as clearly observed in the explosion scenario captured by the high-speed camera. Concrete fragments and metal-ladder residues were observed in the tests.

Figure 7 shows the damage morphology of the concrete blocks under explosion loads at various top spacing distances. As shown, the concrete block's integral damage degree decreased gradually as the top spacing distance increased in this paper. The concrete exhibited an integral fragmentation trend, where collapse originating from the center and propagating to all directions was observed when 30 kg of B-explosive was detonated at a stand-off distance of 500 mm; consequently, several concrete fragments with stripes have resulted. The fragmentation at the center of the

Table 1 Parameters of experimental charges

Materials	Density (g/cm^3)	Detonation velocity (m/s)	Detonation heat (kJ/kg)	Detonation pressure (GPa)
B-explosives	1.63	7900	5180	25.90

Table 2 Parameters of experimental concrete

Materials	Density (g/cm^3)	Poisson's ratio	Compression strength (MPa)	Modulus of elasticity (MPa)
Concrete	2.28	0.20	29.40	3.00×10^4

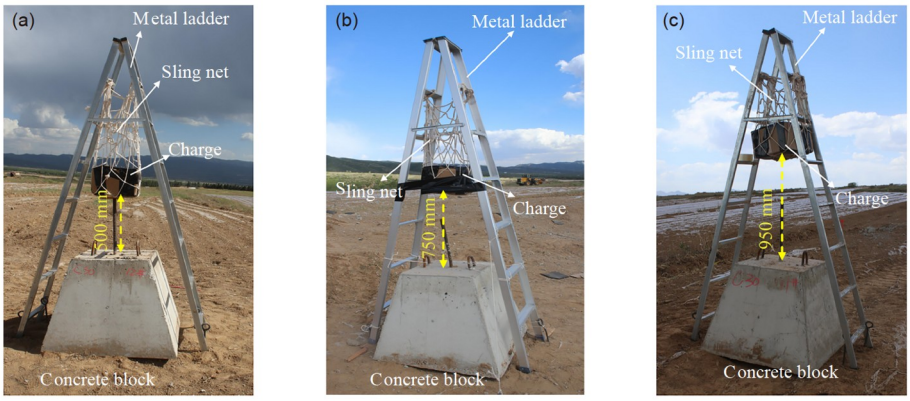

Figure 5 Explosion experiments at various top spacing distances. (a) Top spacing distance is 500 mm; (b) top spacing distance is 750 mm; (c) top spacing distance is 950 mm.

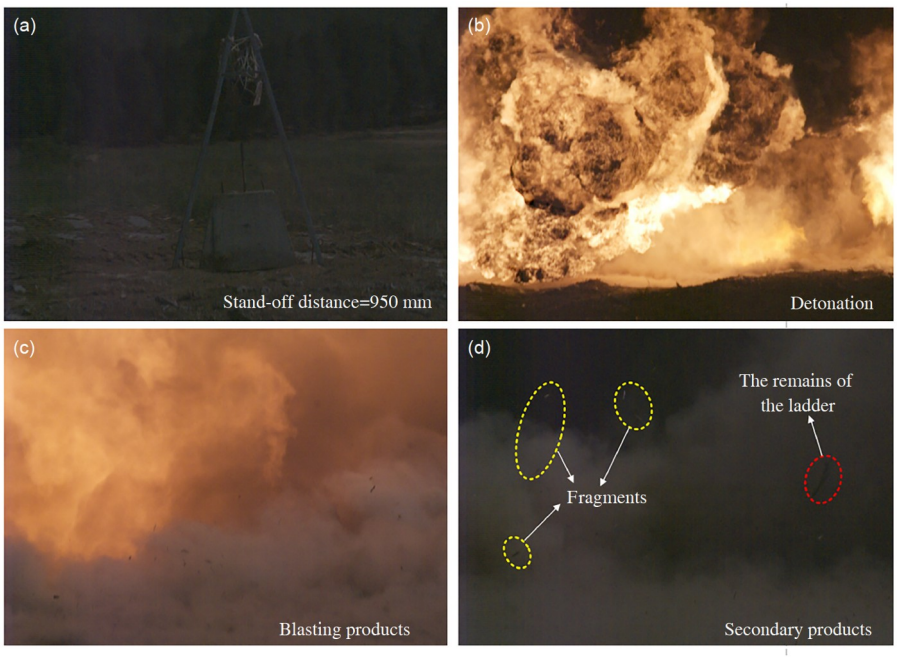

Figure 6 The process of the explosion experiment. (a) The preparation stage of the explosion experiment; (b) the moment of the explosive detonation; (c) the blasting products and smoke were produced; (d) the concrete fragments and the remains of the aluminum alloy herringbone ladder were observed.

block was higher than that around it, and larger concrete fragments were found at all four corners of the block, which were the largest concrete fragments observed (measuring 430 mm × 300 mm × 290 mm). When the 30 kg B-explosive was detonated 750 mm above the block, the concrete fragments were scattered from the center outward, and the concrete was severely fragmented at the center. The larger concrete fragments remained at one of the corners in the block and symmetrical penetrating cracks appeared in the fragments; the largest concrete fragments measured 590 mm × 350 mm × 290 mm. Damage to the concrete block was reduced significantly when 30 kg of B-explosive was detonated 950 mm above the concrete block. The residual height of the concrete block was remarkably higher than that in the previous two tests, and the overall cumulative height of the various large fragments on one side of the block was approximately 800 mm. Several large penetrating cracks were formed, which segmented the block from the center into four damaged areas; here, only one damage zone yielded smaller diameter concrete fragments, while the concrete fragments yielded at other locations were all larger in diameter, of which the largest concrete fragment measured 560 mm × 510 mm × 430 mm.

4.2.2. Collection of concrete fragments

The concrete fragments were collected and screened at the end of the explosion tests to obtain parameter data under various explosion environments. The diameters of the sieves

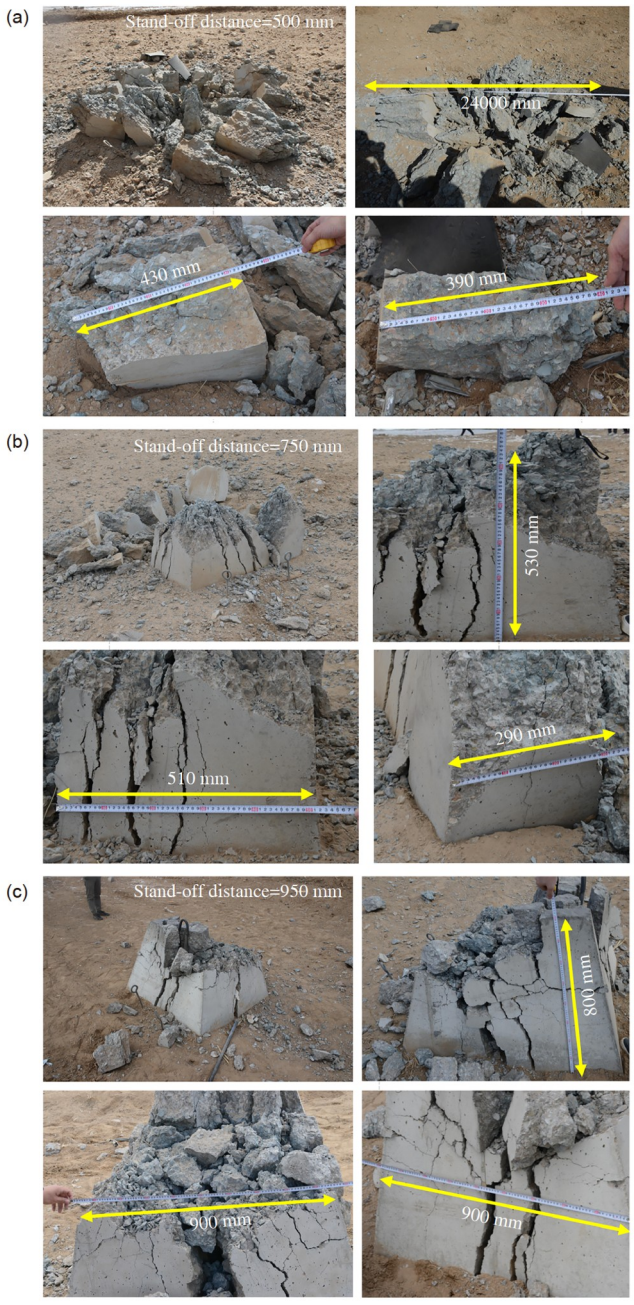

Figure 7 The damage morphology of concrete blocks at various top spacing distances. (a) Top spacing distance = 500 mm; (b) top spacing distance = 750 mm; (c) top spacing distance = 950 mm.

used in this study were 10, 30, 50, 70, and 90 mm, and the sieved concrete fragments were categorized based on the size of the particles as 10–30, 30–50, 50–70, 70–90, 90–150, and ≥ 150 mm. Concrete fragments were recycled and categorized as presented in Figure 8. The recycled fragments were weighed and counted separately at the end of the experiment. Concrete fragments with smaller quantities and larger diameters were counted individually, and the statistics were carried out after mass averaging the concrete fragments with larger quantities and smaller diameters to obtain the experimental data. The experimental data of concrete fragments at various top spacing distances are shown in Table 3.

4.3 Verification of empirical model

An empirical model of fragmentation was established to determine the state of fragmentation for concrete blocks due to explosion loading in detail. Furthermore, the problem pertaining to the quantitative prediction of fragment behavior can be solved using the present model. The fragment behavior of concrete blocks under explosion loads was calculated with the empirical model. The charge mass was set as 30 kg, whereas the top spacing distances were set as 500, 750, and 950 mm. A comparison between the experimental data and the calculation results is shown in Figure 9.

The calculation results were obtained through explosion tests. A comparison between these results and the experimental data shows that the degree of fragmentation of concrete blocks under the action of the blast load reduced gradually as the top spacing distance increased. This occurred because the explosion-wave energy propagation time was extended at a larger stand-off distance, which further attenuated the explosion wave energy. Furthermore, the quantity of concrete fragments with larger diameters was less than the quantity of concrete fragments with smaller diameters, which is consistent with the experimental recycling phenomenon. A comparison of the empirical model calculations of concrete fragments with the experimental recycling data is presented in Table 4. Under the test conditions with top spacing distance was 500 mm, the errors range from the test recovery data to the empirical model calculations were −8.04%–12.75%, with the largest error value of 12.75% in this group. Under the test conditions with top spacing distance of 750 mm, the errors ranging from the test recovery data to the empirical model calculations were −10.16%–14.47%, with the largest error value of 14.47% in this group. Under the test conditions with top spacing distance of 950 mm, the errors ranging from the test recovery data to the empirical model calculations were −14.96%–12.13%, with the largest error value of 14.96% in this group. By comparing the maximum error values of each group, it can be concluded that the maximum error of the calculation was −14.96%. The error in the results of the model calculations may be due to insufficient consideration of the shape parameters of the concrete fragments and the mass-averaging calculation method used in the recycling process. Notably, concrete fragments larger than 150 mm were not considered in this study to verify the calculation because the concrete block within this range was extremely wide and the number of fragments was relatively small. In summary, the fragmentation empirical model coupled with the fracture criterion is used to evaluate the fragment behavior for concrete blocks under explosion loads, thus demonstrating the effec-

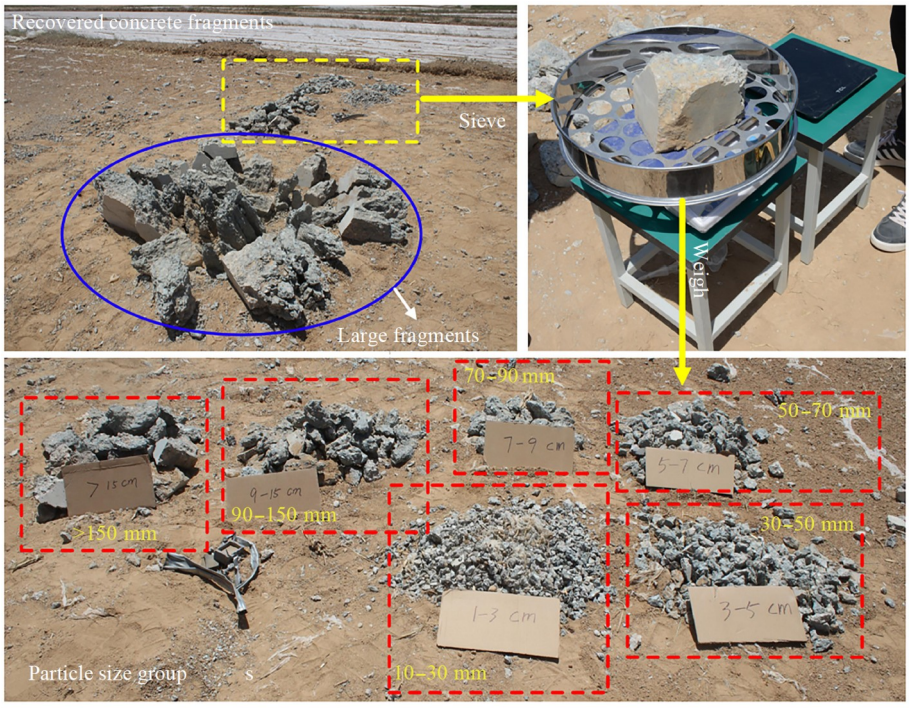

Figure 8 The recycling process and grouping for fragments (the top spacing distance is 500 mm).

Table 3 The experimental data at various top spacing distances

Particle size range (mm)	Top spacing distance is 500 mm, and recycling rate of fragments is 88.69%		Top spacing distance is 750 mm, and recycling rate of fragments is 89.45%		Top spacing distance is 950 mm, and recycling rate of fragments is 90.74%	
	Number	Mass (kg)	Number	Mass (kg)	Number	Mass (kg)
10–30	2553	33.7	1909	25.2	1598	21.2
30–50	423	32.5	305	16.2	272	14.5
50–70	205	24.5	194	24.4	123	16.9
70–90	126	25.7	73	19.1	62	17.9
90–150	102	268.8	76	249.3	52	227.1
≥150	35	393.5	26	451.2	17	499.1

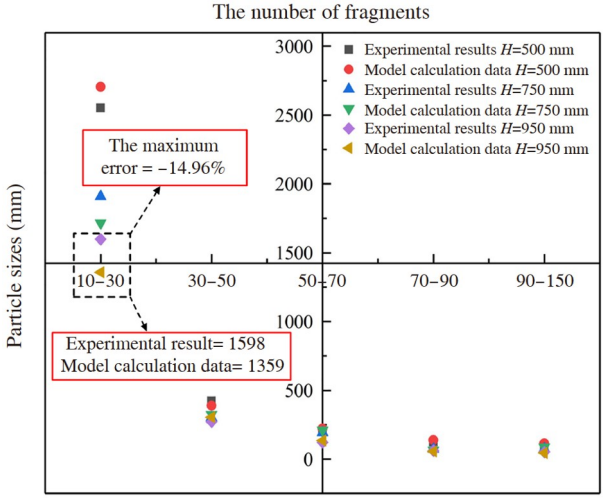

Figure 9 Comparative validation of concrete fragments.

tiveness of the present empirical model.

4.4 Prediction of fragment behavior

The explosion loads were instantaneous and possessed a significant amount of energy; furthermore, the explosion process produces strong light and heavy smoke; hence, capturing the explosion using a high-speed camera or other equipment is challenging. Moreover, a significant amount of time is required to recycle the experimental data, and information regarding the fragment behavior under unknown explosion conditions cannot be acquired. Therefore, an effective fragment empirical model was established to perform the calculation rapidly and accurately. The laws and parameter information of the concrete block under explosion loads at different top stand-off distances and the charge mass

Table 4 Error analysis of empirical model results

Particle sizes range (mm)	Top spacing distance is 500 mm			Top spacing distance is 750 mm			Top spacing distance is 950 mm		
	Test	Model	Error (%)	Test	Model	Error (%)	Test	Model	Error (%)
10–30	2553	2706	5.99	1909	1715	−10.16	1598	1359	−14.96
30–50	423	389	−8.04	305	324	6.23	272	305	12.13
50–70	205	223	8.78	194	213	9.79	123	136	10.57
70–90	126	139	10.32	73	66	−9.59	62	57	−8.06
90–150	102	115	12.75	76	87	14.47	52	46	−11.54

were obtained based on the empirical model presented herein.

4.4.1 Top spacing distances

A fragment empirical model with a coupled fracture criterion for concrete blocks under explosion loads was applied to investigate the fragment behavior of concrete blocks with large dimensions and high strength. The charge mass was 50 kg in the current example, the charge type was B-explosive, and the compressive strength for the concrete blocks was selected to be 40 MPa, and the shape of concrete block was similar to the specimen in the experiment. However, the geometry of the concrete block was larger in this example, with the geometric dimensions of the top surface being 1000 mm × 1000 mm, the bottom surface being 1500 mm × 1500 mm, and the overall vertical dimension of 1000 mm. The locations of the charge placement were set at 400, 600, and 800 mm directly above the concrete block.

The prediction of the concrete fragments at various top spacing distances is shown in Figure 10. The predicted data showed that the number of concrete fragments decreased with an increase in the top spacing distance, and that the total amount of fragments formed was the lowest under the top spacing of 800 mm. Moreover, the smaller the diameter, the higher the amount of concrete fragments, and the amount of fragments decreased rapidly with the gradual increase in the particle size. The fragment behavior patterns of the concrete blocks under explosion loads were consistent with the experimental data.

Furthermore, a percentage distribution for concrete fragments at various top spacing was determined by using the proposed empirical model. The specific percentage distribution of concrete fragments at various explosion conditions is shown in Figure 11. This distribution trend of concrete fragments under the same explosion conditions was similar. The largest proportion was found in the 10–30 mm diameter group, which accounted for approximately 65%–68% of the total amount. Moreover, the proportion observed in the group with diameters of 30–50 mm group was approximately 18%–20%; the proportion found in the group with diameters of 50–70 mm group was approximately 6%–10%; and the proportion observed in the group with diameters of 70–90 mm group was approximately 5%–6%. The lowest proportion of amount was observed in the 90–150 mm group, which was approximately 1%–2%. The percentage distribution with intermediate diameter size

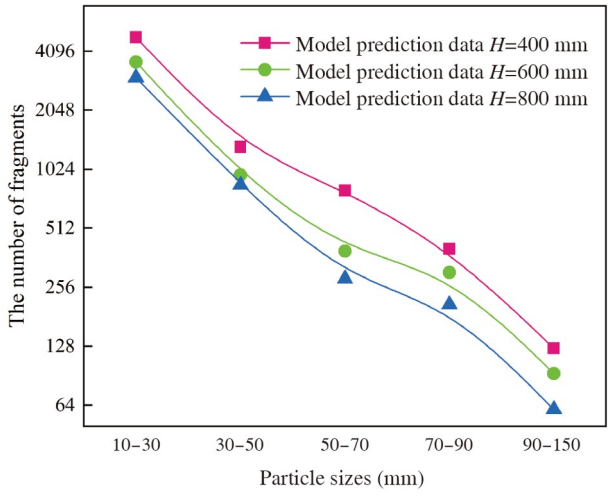

Figure 10 Prediction of fragmentation behavior with various top spacing.

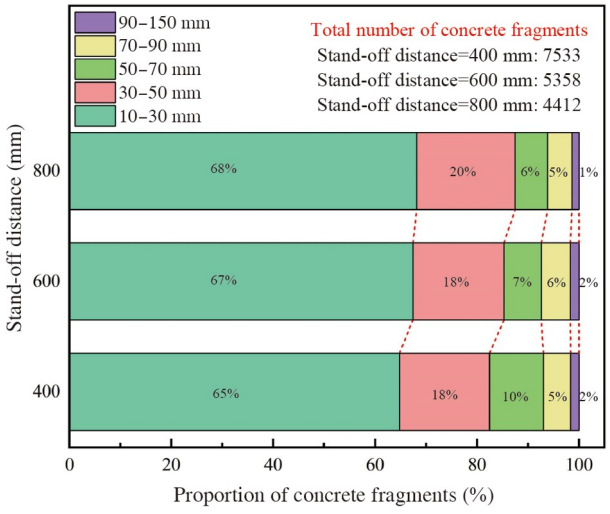

Figure 11 The percentage distribution for fragments at various top spacing.

groups was negatively correlated with the top stand-off distance.

4.4.2 *Charge mass*

Similarly, a fragment empirical model with a coupled fracture criterion was applied to evaluate the fragment behavior of concrete blocks with larger sizes and higher strengths under different charge masses. The charge type, strength, and dimensions of the concrete block in the current example were the same as those in the previous case. The locations of the charge placement were set at 600 mm directly above the concrete block, and the charge masses were set as 10, 30, and 50 kg.

The predicted concrete fragments under different charge masses are presented in Figure 12, which demonstrates that there is an increase in the amount of fragments with the charge mass. Moreover, an increase in the diameter for fragments significantly decreased the amount of concrete fragments within the corresponding group. And the lowest amount of concrete fragments were formed at a charge mass of 10 kg.

Additionally, a percentage distribution for concrete fragments at various charge masses was also determined in conjunction with the proposed empirical model. The specific percentage distribution of concrete fragments under different explosion conditions is presented in Figure 13, which shows that the distribution trend for the fragments at various diameters remained similar in multiple explosion situations. Moreover, the concrete fragments in the 10–30 mm diameter size group accounted for approximately 67%–71% in the three predicted explosion conditions. The lowest proportion of concrete fragments was observed in the 90–150 mm diameter size group, which was approximately 1%–2%. However, the total amount of fragments on the medium diameter group increased slightly with the charge mass. In this case, the proportion observed in the group with diameters of 30–50 mm was approximately 18%–19%; the proportion found in the group with diameters of 50–70 mm was approximately 5%–7%; the proportion observed in the group with diameters of 70–90 mm was approximately 4%–6%.

Impact energy is the direct cause of fragments in concrete blocks and is extremely useful for quantitatively predicting the relationship between impact energy and concrete fragment behavior. The impact energies in the aforementioned explosion scenarios with different stand-off distances and charge masses were calculated separately with the present empirical model. The predicted relationships among the impact energy, concrete fragment particle size, and number of fragments are presented in Figure 14. The maximum amount of fragments was indicated when the impact energy was high and the fragment diameter size was small, as shown by the red area in Figure 14. Subsequently, the number of fragments decreased exponentially as the impact energy

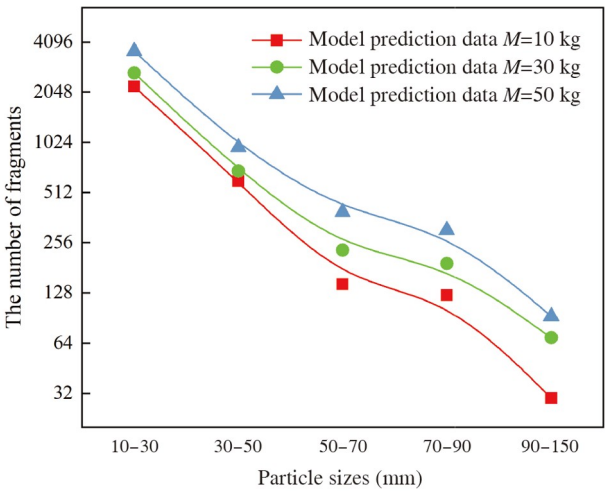

Figure 12 Prediction of fragmentation behavior with different charge masses.

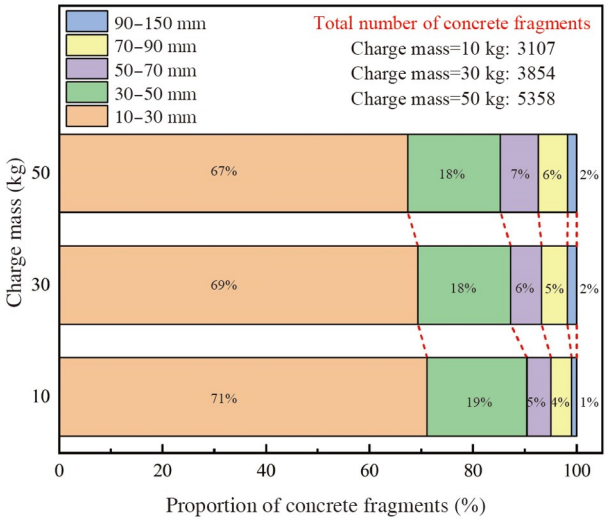

Figure 13 The percentage distribution for fragments at various masses of charge.

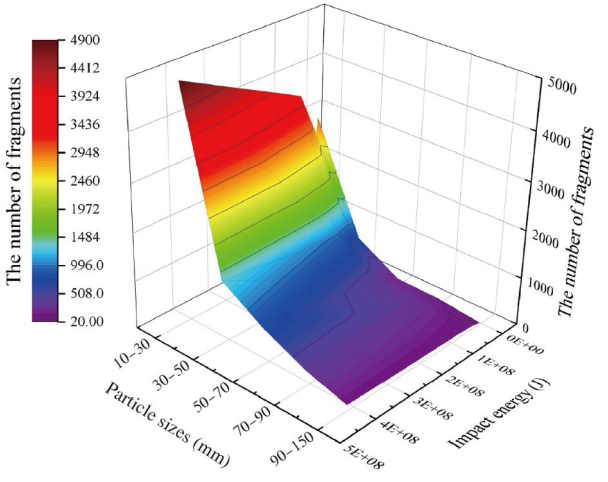

Figure 14 The 3D fitting of fragment parameters.

decreased, and the fragment size increased gradually. Analysis of the calculation results confirms that the results of the present empirical model can be used to clearly reflect the real state of the explosion and to quantitatively determine the parameters of the fragmentation behavior for the concrete members. Therefore, the analysis above shows that the proposed empirical model with a coupled fracture criterion for concrete blocks under explosion loads can reasonably predict the phenomenon of concrete fragments.

5 Conclusions

Fractures and fragments of concrete and other rock-resembling materials are key concerns in the field of ore mining and engineering safety. The degree of rock fragmentation caused by blasting determines the subsequent machining, hauling, and transportation, which directly affect the efficiency and cost of the mining project. Moreover, the concrete fragments generated after the fragmentation of concrete materials pose significant potential risks; thus, an effective assessment of the damage capability of concrete fragments is essential for structural safety and protection. However, it is quite impossible to visualize the response process of concrete structures under explosion loads because of the highly destructive nature of explosion loads and the complexity of the blast physical field. Currently, studies regarding the formation and distribution of concrete structures fragmentation due to explosion loading are limited, and an effective method for quantitative predicting the fragmentation behavior for concrete has not yet been established.

The load-bearing characteristics of concrete members are analyzed on the present research, the Mohr-Coulomb fracture criterion was incorporated into the empirical model to predict the fragment behavior of concrete blocks under explosion loads. Furthermore, the calculation results of the present empirical model were compared and analyzed with the experimental data, and the validity of the empirical model was confirmed. In this study, the propagation and attenuation process of the explosion wave was considered, and a fragment empirical model with a coupled fracture criterion for concrete blocks under explosion loads was established. The main conclusions of this study are as follows.

(1) A method was proposed based on blast theory and the relationship between overpressure and time, which can be used to evaluate the explosion energy productively.

(2) The fragment empirical model with a coupled fracture criterion for concrete blocks under explosion loads was established to quantitatively calculate concrete fragment behavior.

(3) Explosion tests were performed on concrete blocks at various top spacing, and the experimental data on concrete fragmentation were obtained via recycling, sieving, weighing, and counting after the tests.

(4) The empirical model was validated by using experimental data and quantitatively predicted the amount and distribution of fragments in new explosion situations.

This work was supported by the National Natural Science Foundation of China (Grant Nos. 12032006 and 12372350).

1 Sun J, Jia Y, Yao Y, et al. Experimental investigation of stress transients of blasted RC columns in the blasting demolition of buildings. Eng Struct, 2020, 210: 110417
2 Yu Q, Zeng D, Xu X, et al. Experimental and numerical investigation of polymer-reinforced and normal autoclaved aerated concrete masonry walls under large TNT explosive loads. Int J Impact Eng, 2022, 164: 104188
3 Yan J, Liu Y, Xu Z, et al. Experimental and numerical analysis of CFRP strengthened RC columns subjected to close-in blast loading. Int J Impact Eng, 2020, 146: 103720
4 Ning J, Song W, Yang G. Failure analysis of plastic spherical shells impacted by a projectile. Int J Impact Eng, 2006, 32: 1464–1484
5 Xu S, Chen B, Li Q, et al. Experimental and numerical investigations on ultra-high toughness cementitious composite slabs subjected to close-in blast loadings. Cem Concr Compos, 2022, 126: 104339
6 Ren G M, Wu H, Fang Q, et al. Effects of steel fiber content and type on dynamic compressive mechanical properties of UHPCC. Constr Build Mater, 2018, 164: 29–43
7 Ren H, Rong Y, Xu X. Mesoscale investigation on failure behavior of reinforced concrete slab subjected to projectile impact. Eng Fail Anal, 2021, 127: 105566
8 Mu C, Zhou H, Ma H. Prediction method for ground shock parameters of explosion in concrete. Constr Build Mater, 2021, 291: 123372
9 Choi J H, Choi S J, Kim J H J, et al. Evaluation of blast resistance and failure behavior of prestressed concrete under blast loading. Constr Build Mater, 2018, 173: 550–572
10 Zhao C, Lu X, Wang Q, et al. Experimental and numerical investigation of steel-concrete (SC) slabs under contact blast loading. Eng Struct, 2019, 196: 109337
11 Liu L, Zong Z, Gao C, et al. Experimental and numerical study of CFRP protective RC piers under contact explosion. Compos Struct, 2020, 234: 111658
12 Hu Y, Chen L, Fang Q, et al. Blast loading model of the RC column under close-in explosion induced by the double-end-initiation explosive cylinder. Eng Struct, 2018, 175: 304–321
13 Yuan S, Hao H, Zong Z, et al. A study of RC bridge columns under contact explosion. Int J Impact Eng, 2017, 109: 378–390
14 Shi Y C, Sun X Z, Cui J. Reliability analysis of reinforced concrete columns under combined seismic and blast loads. Sci China Tech Sci, 2022, 66: 363–377
15 Zhang C, Gholipour G, Mousavi A A. Blast loads induced responses of RC structural members: State-of-the-art review. Compos Part B-Eng, 2020, 195: 108066
16 Wang H, Wu C, Zhang F, et al. Experimental study of large-sized concrete filled steel tube columns under blast load. Constr Build Mater, 2017, 134: 131–141
17 Su Q, Wu H, Sun H S, et al. Experimental and numerical studies on dynamic behavior of reinforced UHPC panel under medium-range explosions. Int J Impact Eng, 2021, 148: 103761
18 Shi S, Liao Y, Peng X, et al. Behavior of polyurea-woven glass fiber mesh composite reinforced RC slabs under contact explosion. Int J Impact Eng, 2019, 132: 103335
19 Wu H, Peng Y L, Fang Q. Experimental and numerical study of ultra-high performance cementitious composites filled steel tube (UHPCC-FST) subjected to close-range explosion. Int J Impact Eng, 2020, 141: 103569

20 Thai D K, Kim S E. Numerical investigation of the damage of RC members subjected to blast loading. Eng Fail Anal, 2018, 92: 350–367
21 Ruggiero A, Bonora N, Curiale G, et al. Full scale experimental tests and numerical model validation of reinforced concrete slab subjected to direct contact explosion. Int J Impact Eng, 2019, 132: 103309
22 Li Z C, Gu C S, Wang Z Z, et al. On-line diagnosis method of crack behavior abnormality in concrete dams based on fluctuation of sequential parameter estimates. Sci China Tech Sci, 2015, 58: 415–424
23 Zhang Z, Wang X, Deng Y. Dynamic response of square recycled aggregate concrete-filled steel tube columns subjected to close-range blast loads. J Build Eng, 2022, 52: 104427
24 Hao Y, Hao H. Influence of the concrete DIF model on the numerical predictions of RC wall responses to blast loadings. Eng Struct, 2014, 73: 24–38
25 Tu H, Fung T C, Tan K H, et al. An analytical model to predict the compressive damage of concrete plates under contact detonation. Int J Impact Eng, 2019, 134: 103344
26 Wang X, Zhang Z. Residual axial capacity of square recycled aggregate concrete-filled steel tube columns after blast loads. J Build Eng, 2022, 47: 103865
27 Gholipour G, Zhang C, Mousavi A A. Numerical analysis of axially loaded RC columns subjected to the combination of impact and blast loads. Eng Struct, 2020, 219: 110924
28 Ning J, Ren H, Guo T, et al. Dynamic response of alumina ceramics impacted by long tungsten projectile. Int J Impact Eng, 2013, 62: 60–74
29 Li G, Shi X, Gao Y, et al. Reinforcing effects of carbon nanotubes on cement-based grouting materials under dynamic impact loading. Constr Build Mater, 2023, 382: 131083
30 Teng J, Li Z H, Ou J P, et al. Fiber damage analysis model for RC beam-column based on EEP super-convergent computation. Sci China Tech Sci, 2011, 54: 2542–2548
31 Jin Z, Xie F, Yang T, et al. Fractal dimension analysis of concrete specimens under different strain rates. J Build Eng, 2023, 76: 107044
32 Yin X, Li Q, Chen B, et al. An improved calibration of Karagozian & Case concrete/cementitious model for strain-hardening fibre-reinforced cementitious composites under explosion and penetration loadings. Cem Concr Compos, 2023, 137: 104911
33 Shi Y, Wang J, Cui J. Experimental studies on fragments of reinforced concrete slabs under close-in explosions. Int J Impact Eng, 2020, 144: 103630
34 Wang B, Wang P, Chen Y, et al. Blast responses of CFRP strengthened autoclaved aerated cellular concrete panels. Constr Build Mater, 2017, 157: 226–236
35 Xu X, Ma T, Ning J. Failure mechanism of reinforced concrete subjected to projectile impact loading. Eng Fail Anal, 2019, 96: 468–483
36 Xu Y. The fractal evolution of particle fragmentation under different fracture energy. Powder Tech, 2018, 323: 337–345
37 Mei Y, Zhang A, Shen J, et al. A fractal comminution approach for scaling issues of penetration failure of concrete target. Eng Fail Anal, 2022, 140: 106553
38 Zhang P, Gao Z, Shi Y, et al. Effect of large broken stone content on properties of roller compacted concrete based on fractal theory. Constr Build Mater, 2020, 262: 120821
39 Liu Z, Zhao X, Fang H, et al. Investigation on the damage features and dynamic response of reinforced concrete slabs with polyurethane sacrificial cladding under close-range explosions. Constr Build Mater, 2023, 395: 132149
40 Zheng T, Zhang Q, Yuan L, et al. Shape characteristics and crushed law of deep sandstone impact crushed blocks based on digital reconstruction. Int J Impact Eng, 2023, 174: 104525
41 Yang S, Ning J, Xu X. Fragment theoretical model of concrete blocks subjected to blast loads. Int J Impact Eng, 2023, 176: 104562
42 Sun Z, Wang C, Hao X, et al. Quantitative evaluation for shape characteristics of aggregate particles based on 3D point cloud data. Constr Build Mater, 2020, 263: 120156
43 Liu H L, Xiao Y, Liu J Y, et al. A new elliptic-parabolic yield surface model revised by an adaptive criterion for granular soils. Sci China Tech Sci, 2010, 53: 2152–2159
44 Wei X, Ren X. Numerical studies on resistance of concrete target under rigid projectile impact using Perzyna-type visco-damage model. Int J Impact Eng, 2023, 176: 104557
45 Xu X, Ma T, Ning J. Failure analytical model of reinforced concrete slab under impact loading. Constr Build Mater, 2019, 223: 679–691
46 Liu H, Liu J, Zhang S, et al. Experimental study on compression characteristics of fractured soft rock and its Mohr-Coulomb criterion. Theor Appl Fract Mech, 2023, 125: 103820
47 Ning J, Yang S, Ma T, et al. Fragment behavior of concrete slab subjected to blast loading. Eng Fail Anal, 2022, 138: 106370
48 Wu C, Hao H. Modeling of simultaneous ground shock and airblast pressure on nearby structures from surface explosions. Int J Impact Eng, 2005, 31: 699–717
49 Xiong B, Demartino C, Xu J, et al. High-strain rate compressive behavior of concrete made with substituted coarse aggregates: Recycled crushed concrete and clay bricks. Constr Build Mater, 2021, 301: 123875
50 Ning J, Ren H, Li Z, et al. A mass abrasion model with the melting and cutting mechanisms during high-speed projectile penetration into concrete slabs. Acta Mech Sin, 2022, 38: 121597
51 Wang S, Zhang M H, Quek S T. Mechanical behavior of fiber-reinforced high-strength concrete subjected to high strain-rate compressive loading. Constr Build Mater, 2012, 31: 1–11
52 Lepakshi R, Venkatarama Reddy B V. Shear strength parameters and Mohr-Coulomb failure envelopes for cement stabilised rammed earth. Constr Build Mater, 2020, 249: 118708
53 Richart F E, Brandtzg A, Brown R L. A study of the failure of concrete under combined compressive stresses. Bulletin, 1928, 26: 97–102